

Journal of the Pakistan Institute of Chemical Engineers

Journal homepage: www.piche.org.pk/journals



DOI: https://doi.org/10.54693/piche.05311



Mathematical Modeling of Membrane System for Hydrocarbon Gas (C₁ – C₃) Recovery in Polyethylene Plant

O.M. Adeloye^{1*}, E.E Olisa² and P.W. Igbagara³

Submitted: 05/10/2024, Accepted: 10/04/2025, Published: 22/04/2025

Abstract

This study addresses the issue of hydrocarbon loss in petrochemical plants. Three sections were identified in the Indorama polyethylene plant facility in Eleme, Rivers State as locations where hydrocarbons losses occur during the polyethylene production operations. The hollow-fiber membrane system was investigated for the recovery of methane, ethylene, and propylene at these locations. Comprehensive modeling showed that the system was described by eleven coupled ordinary differential equations accounting for mass, energy, and momentum. The model equations were discretized into a set of algebraic equations using the orthogonal collocation method, and the solution to these equations was obtained using the Newton-Raphson method. The results showed a remarkable recovery of methane (~86%), ethylene (~80%), and propylene (~91%) on the shell side while capturing about 82% of carbon dioxide on the fiber side. These results were achieved using the spirobisindane-based ladder polymer (PIM-1) membrane material under 90 bar and 2 bar pressure on the shell and fiber side, respectively, with a membrane area of 6900 m². These results show the effectiveness of the PIM-1 for hydrocarbon gases recovery.

Keywords: Membrane Reactor, Counter Current Flow, Non-Isothermal Model, Isothermal Model, Newton-Raphson, Orthogonal Collocation, Shell and Fiber side

1. Introduction:

The loss of hydrocarbons in petrochemical plants is a crucial problem for petrochemical companies as it directly impacts their profitability and operational costs. According to research conducted by Membrane Technology Research (MTR) Inc., a leading supplier of membrane technology since 1982, polyethylene plants typically experience ethylene and other hydrocarbon feedstock losses amounting to \$1 - \$3 million annually [1]. Hydrocarbon losses significantly affect the profit margin due to recent surge in hydrocarbon prices impacting the production cost of polyethylene which now stands at \$1560 per ton [3].

The Indorama petrochemical plant, in Eleme community of Rivers State, is known to produce 360,000 kilotons of polyethylene annually [2]. For this plant, hydrocarbon losses have significant financial implications.

Three major areas in the Indorama polyethylene production process have been identified as regions where hydrocarbon losses occur. This includes the reactor purge, distillation and purification units. To address this issue, this research investigated the application of membrane separation technology to recover hydrocarbon gases in these units.

Advanced separation procedures significantly depend on membrane technology, which has emerged as the leading solution in several industries. The progress in this technology may be attributed to the ongoing improvement and augmentation of polymer membranes. Polymer membranes are developed to show characteristics of thermal, chemical, and mechanical stability. These properties are vital for their application in industrial settings. These membranes are extensively used in chemical [4], petrochemical [5-8],

¹Department of Chemical Engineering, University of Delta, Agbor, Delta State, Nigeria

²Department of Chemical and Biotechnology Engineering, 2500, boul. de l'Universite, Université de Sherbrooke, Sherbrooke, Quebec, Canada

³Department of Chemical Engineering, Federal University Otuoke, Otuoke, Bayelsa State, Nigeria

^{*}Corresponding Author: olalekan.adeloye (olalekan.adeloye@unidel.edu.ng)

and water treatment [9-11], where it is crucial to handle liquid or gaseous mixtures. The applications include recycling, pollution control, and meeting operating requirements. A significant breakthrough in the application of membrane technology was the successful utilization of the gas permeation process to differentially separate organic vapors from exhaust air. The application focused on managing vapors emitted during the distribution and storage of extremely volatile hydrocarbons [8,12].

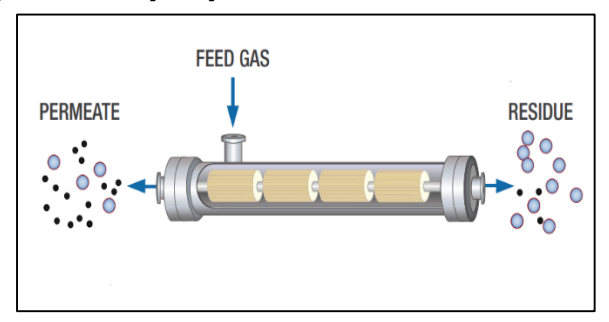


Figure 1: Membrane Separation Process [13]

Industrial applications of membranes include:

- The UOP Separex Membrane Systems which are installed in over 130 units worldwide remove CO₂, H₂S, and water vapor from hydrocarbon streams [14].
- ii. The Cynara membrane units 40 units installed worldwide are used to capture bulk quantities of CO₂ from hydrocarbon gas streams and are even capable of handling condensed liquid hydrocarbons [15].
- iii. Hydrogen upgrading facilities using UOP
 Polysep Membrane Systems by Air Liquide –
 125 units installed worldwide produce a 90 to
 99% hydrogen product stream [13]
- iv. BORSIG Membrane Technology with over 100 units installed worldwide used for the treatment of liquid hydrocarbon streams utilizing a new organic solvent nano-filtration technique. This is now possible at an industrial scale with membrane systems deployed all over the globe [16]
- v. Hydrocarbon recovery from petrochemical plant vents using a membrane system, manufactured by Membrane Technology and Research, Inc.

The selection of membrane materials for hydrocarbon recovery depends on several factors, including permeability, selectivity, stability, and cost. Polymers of Intrinsic Microporosity (PIMs) are a class of polymers

that have intrinsic microporosity, which makes them negligibly permeable to hydrocarbon gases [17]. PIM-1 and PIM-SBF are two examples of PIMs that have shown promise for hydrocarbon separation [18].

Li et al. (2013) conducted a comprehensive investigation on the gas transport properties of PIM-1. The study focused on evaluating the permeability coefficients of ten different gases, including He, H₂, N₂, O_2 , CH_4 , CO_2 , C_2H_4 , C_2H_6 , C_3H_6 , and C_3H_8 , at 25 °C and various pressures ranging from 1 to 10 atm. It was observed that the permeability coefficients of He, H₂, O₂, N₂, CH₄, and CO₂ decreased with increasing transmembrane pressure, aligning with the expected behavior according to the dual-mobility model. On the other hand, the C2 and C3 hydrocarbons exhibited notable plasticization responses. Furthermore, the researchers determined the sorption isotherms for all ten gases using a dual-volume sorption cell, reaching a maximum pressure of 27 atm at 25 °C. In this research, PIM-1 was used due to the availability of gas permeability data for most hydrocarbon gases [19].

In this study, the hollow-fiber membrane and polymer of intrinsic microporosity (spirobisindane-based ladder polymer) known commonly as PIM-1 which has vast applications in the industry was used in this investigative research [20]. The one-dimensional model for the membrane system was developed for mass and energy providing a framework for the development of eleven coupled ordinary differential equations describing the dynamics of the hydrocarbon recovery process. Extensive resources on membrane technology from various literature sources were utilized to obtain the relevant model parameters, and the orthogonal collocation method was then employed as the numerical technique to solve the set of model equations. The results demonstrated an impressive recovery rate for methane, ethylene, and propylene, all achieved on the shell side at 90 bar when utilizing the PIM-1 membrane material.

2. Materials and Methods:

2.1. Model Development:

The hollow fiber system operates in a counter-current flow pattern. The high-pressure multicomponent gas enters the system from the right side and flows in the z direction.

The assumptions made in this study include:

- i. Plug flow condition on the shell side
- ii. Uniform temperature profile on both sides.

- iii. Negligible mass and heat transfer resistance in the boundary layer.
- iv. Solution-diffusion mechanism.
- v. Constant permeance
- vi. Constant membrane thickness.

2.1.1. Material Balance:

Figure 2 presents a schematic representation of the process of gas separation inside the membrane, where the gas feed enters from the right side. The retentate is collected on the left side, and the permeate leaves from the left side of the system.

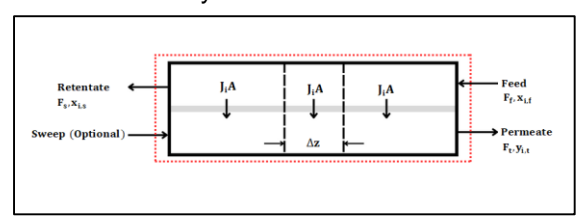


Figure 2: Hollow Fiber Membrane System

Applying the fundamental principles of conservation of mass and energy, the overall material balance equation is expressed:

$$\begin{bmatrix} \text{Rate of inflow} \\ \text{into the system} \end{bmatrix} - \begin{bmatrix} \text{Rate of outflow} \\ \text{from the system} \end{bmatrix} \pm \\ \begin{bmatrix} \text{Rate of generation} \\ \text{or depletion within} \\ \text{the system} \end{bmatrix} = \begin{bmatrix} \text{Rate of accumulation} \\ \text{within the system} \end{bmatrix}$$

$$\tag{1}$$

Considering the absence of reaction and accumulation within the system, (1) simplifies to:

$$\begin{bmatrix} \text{Rate of inflow} \\ \text{into the system} \end{bmatrix} = \begin{bmatrix} \text{Rate of outflow} \\ \text{from the system} \end{bmatrix}$$
 (2)

Overall Material Balance

$$F_f = F_s + F_t \tag{3}$$

For component:

$$F_{f.} x_{i,f} = F_{s.} x_{i,s} + F_{t.} y_{i,t}$$
 (4)

$$\sum x_{i,f} = \sum x_{i,s} = \sum y_{i,t} = 1$$
 (5)

2.1.2. Shell Side Mass Balance:

Figure 3 illustrates the mass balance over the differential element (Δz) on the fiber side.

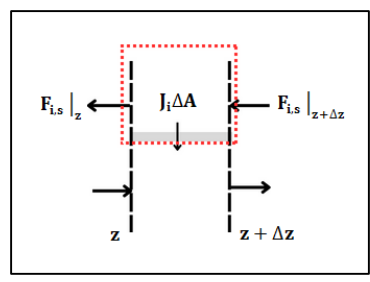


Figure 3: Shell side material balance across the elemental Section

Taking material (component) balance on the shell side, upon mathematical analysis and taking limit as $\Delta z \to 0$, yields:

$$\frac{\mathrm{dF}_{i,s}}{\mathrm{dz}} = N_{\mathrm{T}} \pi D_{\mathrm{o}} J_{i} \tag{6}$$

2.1.3. Fiber Side Mass Balance:

Figure 4 illustrates the mass balance over the differential element (Δz) on the fiber side.

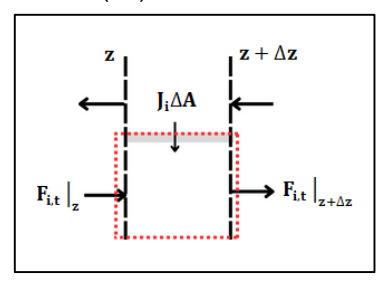


Figure 4: Fiber side material balance across elemental section

Material (component) balance on the fiber side, upon variable separation and taking limit as $\Delta z \rightarrow 0$, yields:

$$\frac{\mathrm{dF}_{i,t}}{\mathrm{dz}} = N_{\mathrm{T}} \pi D_{\mathrm{o}} J_{\mathrm{i}} \tag{7}$$

2.2. Membrane Energy Balance:

2.2.1. Shell Side Energy Balance:

Figure 5 illustrates the energy balance over the differential element (Δz) on the shell side.

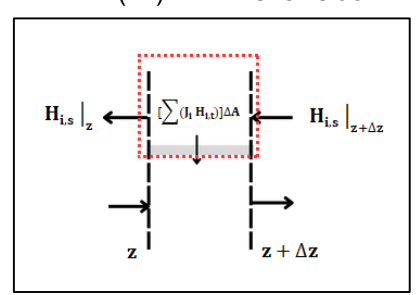


Figure 5: Shell side energy balance across elemental section

Taking energy balance on the shell side with mathematical analysis and taking limit as $\Delta z \rightarrow 0$:

$$\frac{dT_{s}}{dz} = \frac{N_{T}\pi D_{o} \cdot \sum_{i=1}^{N} J_{i} \cdot C_{p_{i}} (T_{s} - T_{t})}{\sum_{i=1}^{N} F_{i,s} \cdot C_{p_{i}}}$$
(8)

2.2.2. Fiber Side Energy Balance:

Figure 6 illustrates the energy balance over the differential element (Δz) on the fiber side.

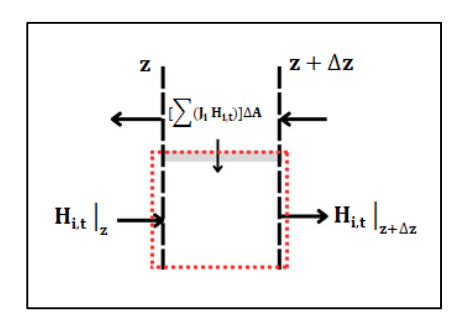


Figure 6: Fiber side energy balance across elemental section

Upon variable separation and taking the limit as $\Delta z \rightarrow 0$:

$$\frac{dT_{t}}{dz} = \frac{N_{T}\pi D_{0} \cdot \sum_{i=1}^{N} J_{i} \cdot C_{p_{i}} (T_{s} - T_{t})}{\sum_{i=1}^{N} F_{i,t} \cdot C_{p_{i}}}$$
(9)

2.3. Pressure Drop on Fiber Side:

The pressure drop on the fiber side have been derived by Helmersen as [21]:

$$P_{t} = \frac{{}^{128\mu zRT_{t}}}{{}^{N_{T}\pi D_{c}}{}^{4}.P_{t}}.\sum_{i=1}^{N}F_{i,t}$$
 (10)

Taking a balance over a small element Δz and upon variable separation yields

$$\frac{dP_{t}}{dz} = -\frac{128\mu.RT_{t}}{N_{T}\pi D_{c}^{4}.P_{t}}.\sum_{i=1}^{N} F_{i,t}$$
 (11)

Isothermal Model:

The shell side =
$$\begin{cases} \frac{dF_{i,s}}{dz} = N_T \pi D_o J_i & (12) \end{cases}$$
 The fiber side =
$$\begin{cases} \frac{dF_{i,t}}{dz} = N_T \pi D_o J_i \\ \frac{dP_t}{dz} = -\frac{128\mu.RT_t}{N_T \pi D_c^4.P_t} \cdot \sum_{i=1}^{N} F_{i,t} \end{cases}$$
 (13)

The equation representing the mathematical model for the material, momentum, and energy balance in the membrane system is derived as follows:

Non-isothermal Model:

$$\text{The shell side} = \begin{cases} \frac{dF_{i,s}}{dz} = N_{T}\pi D_{o} J_{i} \\ \frac{dT_{s}}{dz} = \frac{N_{T}\pi D_{o} \cdot (T_{s} - T_{t})}{\sum_{i=1}^{N} F_{i,s} \cdot C_{p_{i}}} \sum_{i=1}^{N} C_{p_{i}} J_{i} \end{cases}$$
 (14)
$$\text{The fiber side} = \begin{cases} \frac{dF_{i,t}}{dz} = N_{T}\pi D_{o} J_{i} \\ \frac{dP_{t}}{dz} = -\frac{128\mu \cdot RT_{t}}{N_{T}\pi D_{c}^{4} \cdot P_{t}} \cdot \sum_{i=1}^{N} F_{i,t} \\ \frac{dT_{t}}{dz} = \frac{N_{T}\pi D_{o} \cdot (T_{s} - T_{t})}{\sum_{i=1}^{N} F_{i,t} \cdot C_{p_{i}}} \sum_{i=1}^{N} C_{p_{i}} \cdot J_{i} \end{cases}$$

2.4. Definition of Parameters:

2.4.1. Flux (J_i):

This is a driving force across the membrane provided by the partial pressure gradient at the shell side and fiber side of the membrane. The gas separation mechanism employed in this research was governed by the solution diffusion model of Baker as [22]:

$$J_{i} = \frac{Q_{i}}{\kappa} (P_{s} x_{i} - P_{t} y_{i})$$
 (16)

$$x_i = \frac{F_{s.x_i}}{\sum_{i=1}^{N} F_{s.x_i}}; \quad y_i = \frac{F_{t.y_i}}{\sum_{i=1}^{N} F_{t.y_i}}$$
 (17)

2.4.2. Dimensionless Variables:

The model equations developed are put in the dimensionless form by introducing the following dimensionless variables.

Dimensionless Flow rate $(F_{i,s}^*$ and $F_{i,t}^*)$

$$F_{s}^{*} = \frac{F_{s}x_{i}}{(\sum_{i=1}^{N} F_{s}.x_{i})_{R}}; \quad F_{t}^{*} = \frac{F_{t}y_{i}}{(\sum_{i=1}^{N} F_{s}.x_{i})_{R}}$$
(18)

$$F_s = F_s^* \cdot (\sum_{i=1}^N F_s \cdot x_i)_R; \quad F_{i,t} = F_t^* \cdot (\sum_{i=1}^N F_s \cdot x_i)_R$$
(19)

$$F_{s.} x_{i} = F_{i,s}; F_{t.} y_{i} = F_{i,t}$$
 (20)

$$F_{i,s}^* = (F_s, x_i)^* = F_s, x_i^*;$$

$$F_{it}^* = (F_s, y_i)^* = F_t, y_i^*$$
 (21)

$$F_{s} = F_{s}.x_{i}^{*} (\sum_{i=1}^{N} F_{s}.x_{i})_{R}; \quad F_{t} = F_{t}.y_{i}^{*} (\sum_{i=1}^{N} F_{s}.x_{i})_{R}$$
(22)

Dimensionless Length (ξ)

$$\xi = \frac{z}{L_R}; \tag{23}$$

$$z = \xi. L_R \tag{24}$$

Dimensionless Pressure (P_s^* and P_t^*)

$$P_{s}^{*} = \frac{P_{s}}{P_{p}}; P_{t}^{*} = \frac{P_{t}}{P_{p}}$$
 (25)

$$P_s = P_s^* . P_R; P_t = P_t^* . P_R$$
 (26)

Dimensionless Temperature (T_s^* and T_t^*)

$$T_s^* = \frac{T_s}{T_s}; T_t^* = \frac{T_t}{T_s}$$
 (27)

$$T_s = T_s^* . T_R; T_t = T_t^* . T_R$$
 (28)

Substituting these dimensionless parameters into the model equations yields:

Dimensionless Isothermal Model:

The shell side =
$$\left\{ \frac{dF_s x_i^*}{d\xi} = \alpha \left[\frac{Q_i}{\delta} \left(P_s^* x_i^* - P_t^* y_i^* \right) \right]$$
 (29)

The fiber side =
$$\begin{cases} \frac{dF_{t}.y_{i}^{*}}{d\xi} = \alpha \left[\frac{Q_{i}}{\delta} (P_{s}^{*}x_{i}^{*} - P_{t}^{*}y_{i}^{*}) \right] \\ \frac{dP_{t}^{*}}{d\xi} = \beta \frac{\sum_{i=1}^{N} (F_{t}.y_{i})^{*}}{P_{t}^{*}} \end{cases}$$
(30)

$$\alpha = \frac{{{N_T}{\pi }{D_o}{L_R}{P_R}}}{{\left({\sum_{i = 1}^N ({F_S}.{x_i})_R} \right)}}; \quad \beta = - \frac{{{128}{L_R}{\mu R}\sum_{i = 1}^N ({F_S}.{x_i})_R}}{{P_R^2.{N_T}{\pi }{D_c}^4}}$$

Dimensionless Non-isothermal Model:

The shell side =

$$\begin{cases} \frac{dF_{,s}.x_{i}^{*}}{d\xi} = \alpha \left[\frac{Q_{i}}{\delta} \left(P_{s}^{*}x_{i}^{*} - P_{t}^{*}y_{i}^{*} \right) \right] \\ \frac{dT_{s}^{*}}{d\xi} = \gamma . \frac{\left(T_{s}^{*} - T_{t}^{*} \right)}{\sum_{i=1}^{N} \left(F_{s}.x_{i} \right)^{*}C_{p_{i}}} . \sum_{i=1}^{N} C_{p_{i}} \left[\frac{Q_{i}}{\delta} \left(P_{s}^{*}x_{i}^{*} - P_{t}^{*}y_{i}^{*} \right) \right] \end{cases} \tag{31} \end{cases}$$

The fiber side =

$$\begin{cases} \frac{dF_{t}.y_{i}^{*}}{d\xi} = \alpha \left[\frac{Q_{i}}{\delta} \left(P_{s}^{*}x_{i}^{*} - P_{t}^{*}y_{i}^{*} \right) \right] \\ \frac{dP_{t}^{*}}{d\xi} = \beta^{*} \frac{T_{t}^{*}}{P_{t}^{*}} \cdot \sum_{i=1}^{N} (F_{t}.y_{i})^{*} \\ \frac{dT_{t}^{*}}{d\xi} = \gamma \cdot \frac{(T_{s}^{*} - T_{t}^{*})}{\sum_{i=1}^{N} (F_{t}.y_{i})^{*} C_{p_{i}}} \cdot \sum_{i=1}^{N} C_{p_{i}} \left[\frac{Q_{i}}{\delta} \left(P_{s}^{*}x_{i}^{*} - P_{t}^{*}y_{i}^{*} \right) \right] \\ \beta^{*} = \frac{128L_{R}\mu RT_{R}}{P_{R}^{2}N_{T}\pi D_{c}^{4}}; \quad \gamma = \frac{N_{T}L_{R}\pi D_{o}.P_{R}}{\sum_{i=1}^{N} (F_{s}.x_{i})_{R}} \end{cases}$$

2.5. Performance Parameters:

The separation and economic performance of the membrane-based separation process depend on several parameters. An analysis of the correlation between input conditions, operating variables, and output conditions are carried out. In membrane gas separation, the main performance indicators are:

Recovery (R):

This is the ratio of fiber side condition at the outlet of the system to the condition of the feed at the inlet for a given component i.

Mathematically defined as:

$$R = \frac{F_{t}(L)y_{i,t}(L)}{F_{f}y_{i,f}}$$
 (33)

Purity (P):

This is the composition of a given component i in the fiber side exit stream.

Mathematically defined as:

$$P = y_{i,t}(L) \tag{34}$$

Separation Factor (S):

Mathematically defined as:

$$S = \frac{y_{i,t}(L)[1 - y_{i,s}(L)]}{y_{i,s}(L)[1 - y_{i,t}(L)]}$$
(35)

2.6. Case Study:

The vent gas is multi-component mixture of C_2H_4 , CO_2 , CH_4 , C_3 , and other heavier hydrocarbons from the polyethylene plant effluent unit (see Table 1) is introduced into a hollow fiber membrane as depicted in Fig. 1. Neglecting the heavier components and considering only C_2H_4 , CO_2 , CH_4 , and C_3 , the model equation for each component in the system is derived as follows:

Shell Side:

$$\frac{dF_{S}.x_{1}^{*}}{d\xi} = \alpha \left[\frac{Q_{1}}{\delta} (P_{S}^{*}x_{1}^{*} - P_{t}^{*}y_{1}^{*}) \right] \qquad (36)$$

$$\frac{dF_{S}.x_{2}^{*}}{d\xi} = \alpha \left[\frac{Q_{2}}{\delta} (P_{S}^{*}x_{2}^{*} - P_{t}^{*}y_{2}^{*}) \right] \qquad (37)$$

$$\frac{dF_{S}.x_{3}^{*}}{d\xi} = \alpha \left[\frac{Q_{3}}{\delta} (P_{S}^{*}x_{3}^{*} - P_{t}^{*}y_{3}^{*}) \right] \qquad (38)$$

$$\frac{dF_{S}.x_{4}^{*}}{d\xi} = \alpha \left[\frac{Q_{3}}{\delta} (P_{S}^{*}x_{4}^{*} - P_{t}^{*}y_{4}^{*}) \right] \qquad (39)$$

$$\frac{dT_{s}^{*}}{d\xi} = \gamma \cdot \frac{(T_{s}^{*} - T_{t}^{*})}{\sum_{i=1}^{5} (F_{s} \cdot x_{i})^{*} C_{p_{i}}} \cdot \sum_{i=1}^{5} C_{p_{i}} \left[\frac{Q_{i}}{\delta} \left(P_{s}^{*} x_{i}^{*} - P_{t}^{*} y_{i}^{*} \right) \right]$$

$$(40)$$

Fiber Side:

$$\frac{dF_{t}.y_{1}^{*}}{d\xi} = \alpha \left[\frac{Q_{1}}{\delta} \left(P_{s}^{*} x_{1}^{*} - P_{t}^{*} y_{1}^{*} \right) \right]$$
 (41)

$$\frac{dF_{t}.y_{2}^{*}}{d\xi} = \alpha \left[\frac{Q_{2}}{\delta} \left(P_{s}^{*} x_{2}^{*} - P_{t}^{*} y_{2}^{*} \right) \right]$$
 (42)

$$\frac{dF_{t}.y_{3}^{*}}{d\xi} = \alpha \left[\frac{Q_{3}}{\delta} \left(P_{s}^{*} x_{3}^{*} - P_{t}^{*} y_{3}^{*} \right) \right]$$
 (43)

$$\frac{dF_{t}.y_{4}^{*}}{d\xi} = \alpha \left[\frac{Q_{4}}{\delta} \left(P_{s}^{*} x_{4}^{*} - P_{t}^{*} y_{4}^{*} \right) \right] \tag{44}$$

$$\frac{dP_t^*}{d\xi} = \beta^* \frac{T_t^*}{P_t^*} \cdot \sum_{i=1}^4 (F_t, y_i)^*$$
 (45)

$$\frac{dT_t^*}{d\xi} = \gamma \cdot \frac{(T_s^* - T_t^*)}{\sum_{i=1}^4 (F_t \cdot y_i)^* C_{p_i}} \cdot \sum_{i=1}^4 C_{p_i} \left[\frac{Q_i}{\delta} (P_s^* x_i^* - P_t^* y_i^*) \right]$$
(46)

2.7. Model Parameters:

2.7.1. Composition of the Vent Gas Stream:

Table 1: Composition of the vent gas Indorama PE plant [23]

Component	Mole fraction
C_2H_4	0.375
CH_4	0.125
CO_2	0.25
C_3	0.25

2.7.2. Physical Properties:

Table 2: Specific heat capacities and viscosities of components at standard temperature and pressure (STP) [24]

Component	Specific heat capacity [JK ⁻¹ kmol ⁻¹]	Viscosity [μ. Pa s]		
C_2H_4	52.50	88.5		
CO_2	37.13	15.8		
CH ₄	35.69	9.9		
C ₃₊	127.6	525.5		

2.7.3. Membrane Material and Permeability (Q_i):

Table 3: Gas permeance (in Barrer) in polymer membrane [25]

Polymer Types	Description	Extended Description	C ₂ H ₄	CO ₂	CH ₄	C ₃₊	Ref
		Polymer with Intrinsic					
Polymer with free volume	PIM – 1	Microporosity	535	5303	320	205	Li et al.
		(spirobisindane-based					(2013)
		ladder polymer)					

(1 Barrer =
$$\approx 3.348 \times 10^{-19} \frac{\text{kmol}}{\text{m.s.Pa}} = 3.348 \times 10^{-16} \frac{\text{kmol}}{\text{m.s.KPa}} = 1.2053 \times 10^{-12} \frac{\text{kmol}}{\text{m.hr.KPa}}$$
)

2.7.4. Operating Condition:

Table 4: Operating conditions

Parameter	Value	Unit
Temperature	50	°C
Shell-side pressure	5 - 90	Bar
Fiber-side pressure	2	bar
Flow rate of the feed	100000	mol/h

2.7.5. Membrane Specification:

Table 5: Specification of a Hollow fiber membrane system [22]

Parameter	Value	Unit
Diameter	0.2	m
Length	1	M
Internal		
diameter of	200	Mm
fibers		
External		
diameter of	250	Mm
fibers		
Thickness of	2	Mm
membrane	2	IVIIII
Number of	_	
fibers (1000)		

2.8. Initial Condition:

$$z = 1; x_{i,s} = \begin{cases} x_{C_2H_2,0} = 0.375 \\ x_{CO_2,0} = 0.125 \\ x_{CH_4,0} = 0.25 \end{cases};$$

$$x_{C_{3+},0} = 0.25$$

$$z = 0; y_{i0,t} = \begin{cases} y_{C_2H_2,0} = 0 \\ y_{CO_2,0} = 0 \\ y_{CH_4,0} = 0 \\ y_{C_{3+},0} = 0 \end{cases}$$

$$(47)$$

2.9. Solution Technique:

The orthogonal collocation method was employed as a solution technique to transform the model equations into a set of algebraic expressions. This set of algebraic equations were solved using the MathWorks Computational Tool.

2.9.1. Orthogonal Collocation Method:

The orthogonal collocation method is a numerical technique for solving boundary value problems by approximating the solution using interpolating polynomials and ensuring that the solution satisfies the differential equation and boundary conditions at specific collocation points chosen strategically. This method is particularly useful when dealing with differential equations that cannot be solved analytically.

The system's dimensionless model equations presented earlier correspond to the boundary value problem expressed by the general first order differential equations within the range of 0 < z < 1, as depicted thus.

$$\psi\left[\frac{\mathrm{dX}}{\mathrm{dz}}, X, z\right] = 0 \tag{48}$$

Subject to these boundary conditions:

$$f_1[X, 0] = 0$$

 $f_2[X, 1] = 0$

Representing the proposed approximate solution of the problem by the interpolating polynomial X(z), then the values of the solutions at the collocation points can be expressed as follows:

$$\begin{split} X(z) &= \alpha_0 + \alpha_1 z + \alpha_2 z^2 + \dots + \alpha_n z^n \\ X(z_1) &= \alpha_0 + \alpha_1 z_1 + \alpha_2 z_1^2 + \dots + \alpha_n z_1^n \\ X(z_2) &= \alpha_0 + \alpha_1 z_2 + \alpha_2 z_2^2 + \dots + \alpha_n z_2^n \\ \vdots \\ X(z_{n+1}) &= \alpha_0 + \alpha_1 z_{n+1} + \alpha_2 z_{n+1}^2 + \dots + \alpha_n z_{n+1}^n \end{split}$$

The solution can be transformed into the matrix form as:

$$\begin{bmatrix} 1 & z_{1} & \cdots & z_{1}^{n} \\ 1 & z_{2} & \cdots & z_{2}^{n} \\ 1 & z_{2} & \cdots & z_{3}^{n} \\ \vdots & \vdots & \cdots & \vdots \\ 1 & z_{n+1} & \cdots & z_{n+1}^{n} \end{bmatrix} \cdot \begin{bmatrix} \alpha_{0} \\ \alpha_{1} \\ \alpha_{2} \\ \vdots \\ \alpha_{n} \end{bmatrix} = \begin{bmatrix} X_{1} \\ X_{2} \\ X_{3} \\ \vdots \\ X_{n+1} \end{bmatrix} (50)$$

This can be expressed as:

$$A. \theta = X \tag{51}$$

Expressing the vector matrix θ in terms of the matrix X, which contains the unknowns.

$$\theta = A^{-1}.X \tag{52}$$

Where
$$X_i = X(z_i)$$

To discretize the first derivative in the problem and evaluate it at the collocation points, the first-order

derivative of the interpolating polynomial is deduced from equation (50) as follows:

$$\frac{\mathrm{d}X(z)}{\mathrm{d}z} = 0 + \alpha_1 + 2\alpha_2 z + \dots + n\alpha_n z^{n-1}$$
 (53)

Equation (53) can be expressed in the form:

$$\frac{\mathrm{dX}(z)}{\mathrm{dz}} = \begin{bmatrix} 0 & 1 & 2z & \dots & nz^{n-1} \end{bmatrix} \cdot \begin{bmatrix} \alpha_0 \\ \alpha_1 \\ \vdots \\ \alpha_n \end{bmatrix}$$

$$\frac{dX(z)}{dz} = [0 \quad 1 \quad 2z \quad ... \quad nz^{n-1}].A^{-1}.X (54)$$

Hence, for the i-th collocation point,

$$\frac{dX(z_i)}{dz} = \begin{bmatrix} 0 & 1 & 2z_i & ... & nz_i^{n-1} \end{bmatrix}. A^{-1}. X$$
 (55)
$$\frac{dX(z_i)}{dz} = \begin{bmatrix} S^{(i)} \end{bmatrix}^T. X$$
 (56)

The true solution for the ordinary differential equation must be valid at all designated collocation points, where it is ensured that the residual $(R_{\rm i})$ becomes zero at each of these points. These specific collocation points were strategically selected as the roots of the shifted Legendre polynomial.

This implies that:

$$R_{i} = \psi \left[\frac{dX_{i}}{dz}, X_{i}, z_{i} \right] = 0$$
 (57)
For $i = 2, 3, ..., n$

$$\psi[S. X, X_i, z_i] = 0 \tag{58}$$

Introducing (n+1) by (n+1) vector matrix, denoted as S.

$$S = \begin{bmatrix} \begin{bmatrix} S^{(1)} \end{bmatrix}^{T} \\ \begin{bmatrix} S^{(2)} \end{bmatrix}^{T} \\ \vdots \\ \begin{bmatrix} S^{(n+1)} \end{bmatrix}^{T} \end{bmatrix} = \begin{bmatrix} 0 & 1 & \dots & nz_{1}^{n} \\ 0 & 1 & \dots & nz_{2}^{n} \\ \vdots & \vdots & \dots & \vdots \\ 0 & 1 & \dots & nz_{n+1}^{n} \end{bmatrix} . A^{-1} (59)$$

$$S = C. A^{-1}$$
(60)

Equation (58) comprises (n-1) equations, and the remaining two equations arise from boundary conditions, resulting in a total of (n+1) equations and (n+1) unknown. These systems of equations must be solved simultaneously for linearity or numerically if they exhibit non-linearity.

3. Results and Discussion:

The results deduced from the simulation of the developed models for membrane systems for hydrocarbon recovery are discussed with a focus on analyzing the effect of key process conditions on the recovery of hydrocarbon and the overall efficiency of the membrane system. The results obtained for the recovery of hydrocarbons via the simulation of the developed models at a shell side pressure of 90 bar and fiber side pressure of 2 bar using a membrane area of 6900 m² are shown in Table 6.

Table 6: Simulation Result

Feed Mole Comp. Fraction	Feed (mol/h)	Shell Side Recovery	Fiber Side Recovery	Permeate (mol/h)	Retentate (mol/h)	Purity	
	((%)	(%)	((
Carbon dioxide	0.25	25000	0.1942	0.8058	20144	4856	0.0710
Methane	0.125	12500	0.8673	0.1327	1659	10841	0.1585
Ethylene	0.375	37500	0.7982	0.2018	7569	28831	0.4375
C3	0.25	25000	0.9115	0.0885	2212	22788	0.3331
Total		100000			31584	67316	

3.1. Total Flow Rate in the Shell and Fiber Side against Length:

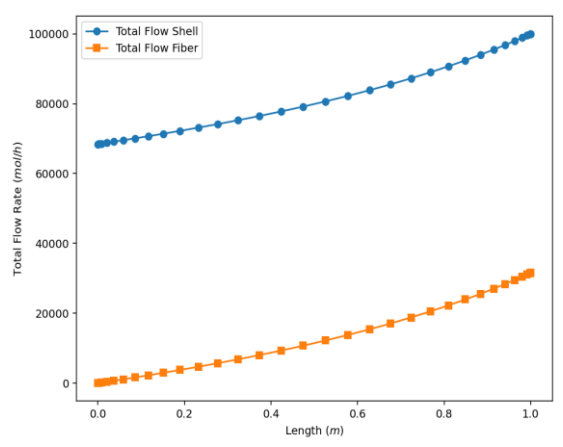


Figure 7: Total flow rate on the shell and fiber side vs. length

3.2. Flow Rate of Component in the Shell and Fiber Side against Length:

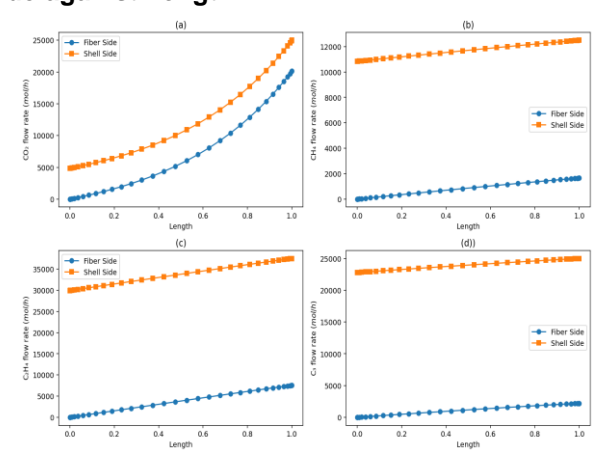


Figure 8: Flow Rate of Component vs length

3.3. Influence of Membrane Area:

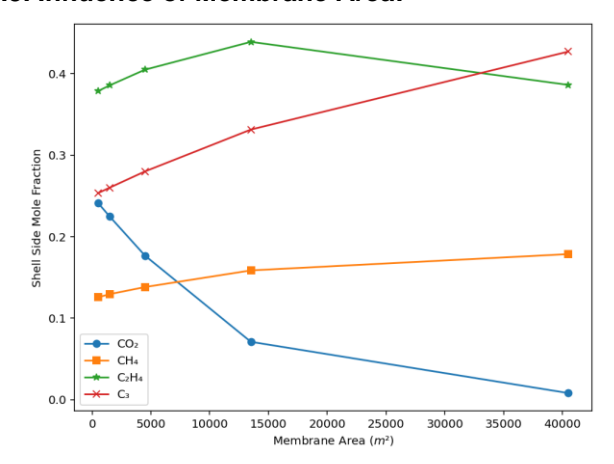


Figure 9: Effect of membrane area on shell side composition

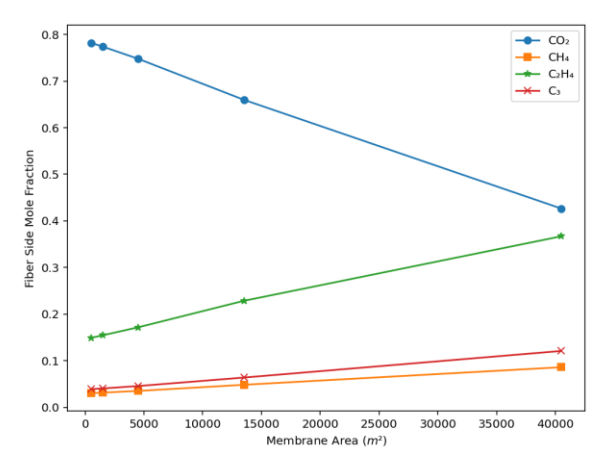


Figure 10: Effect of membrane area on fiber side composition

3.4. Influence of Feed Pressure:

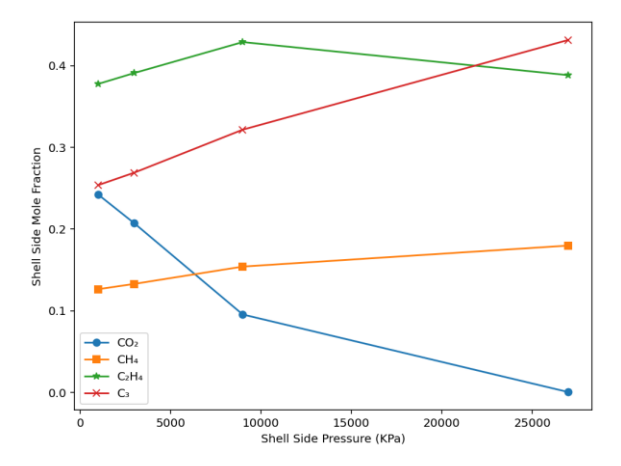


Figure 11: Effect of feed pressure on shell side composition.

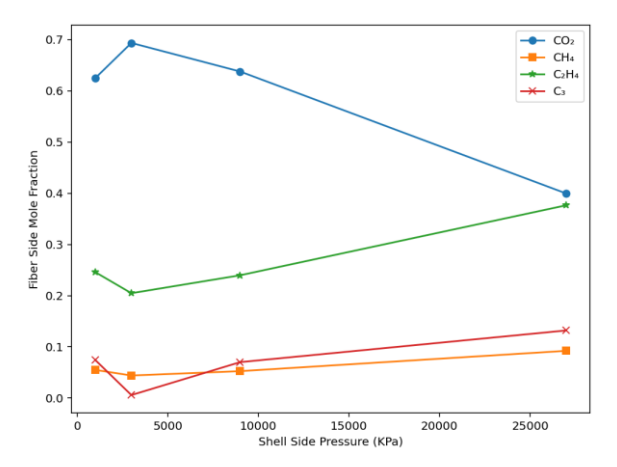


Figure 12: Effect of feed pressure on fiber side composition

3.5. Influence of Membrane Area and Pressure on Recovery:

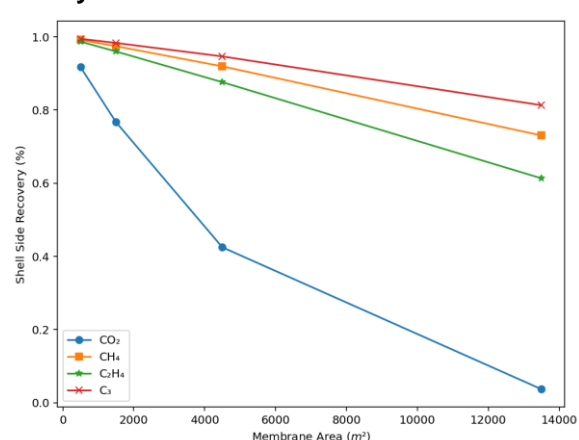


Figure 13: Effect of Membrane Area on recovery

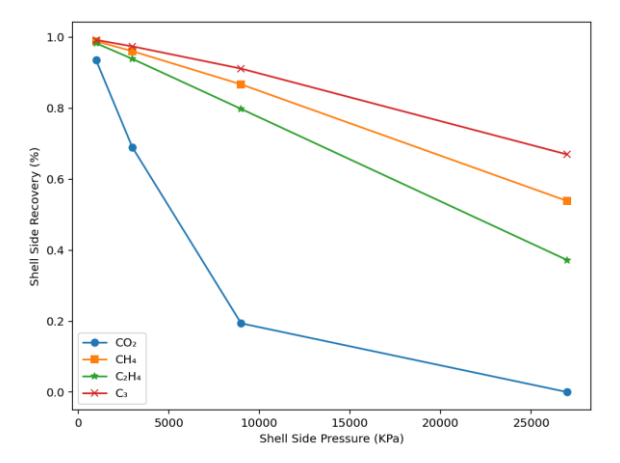


Figure 14: Effect of feed pressure on recovery

4. Conclusion:

The research study addresses the need to mitigate hydrocarbon losses in polyethylene plants by developing an economical gas recovery alternative that will be integrated into the plant to reduce the loss of

methane, ethylene, and propylene. The Indorama polyethylene plant was used as a case study in this research. The one-dimensional mathematical models for mass and energy were developed for the membrane system by employing the fundamental principles of conservation of mass and energy. Eleven coupled ordinary differential equations were obtained that described the dynamics of the process and predicted the recovery rates of methane, ethylene, and propylene at various process conditions.

This study contributes a solution to the growing operational constraint that polyethylene companies annually during polyethylene incur production. The findings of this research provide evidence that membrane systems have the potential to recover hydrocarbon gases, which when utilized can solve the issue of hydrocarbon losses in petrochemical plants. This research highlights the promise membrane recovery technology holds if applied within the petrochemical industry landscape and supports the advancement and commercialization of membrane technology for hydrocarbon recovery

Funding Sources

This research did not receive any specific grant from funding agencies in the public, commercial, or not-forprofit sectors.

Conflicts of Interest

The authors declare no conflict of interest. All authors have read and agreed to the published version of the manuscript.

Nomenclature

 C_{p_i} : Specific heat capacity of component i in the feed (J/(kmol. K))

D_c: Internal diameter of fiber (m)

D_o: External diameter of fiber (m)

F_f: Total molar flow rate in feed stream (kmol/hr)

 $F_{i,s} \hbox{: Molar flow rate of component i in the retentate (shell side) (kmol/hr)} \\$

 $F_{i,t}$: Molar flow rate of component i in the permeate side (fiber side) (kmol/hr)

 F_t : Total molar flow rate in the permeate side (fiber side) (kmol/hr)

 F_s : Total molar flow rate in the retentate (shell side) (kmol/hr)

 J_i : Molar flux across the membrane for each component (kmol/(hr. m²))

L_R: Model Length (m)

N_T: Number of transfer unit

P_R: Model Pressure (KPa)

P_t: Total pressure fiber side (KPa)

P_s: Total pressure in the shell side (KPa)

 Q_i : Permeability of component i in each membrane (kmol/(m. hr. KPa))

R_i: Residual

T_R: Model Temperature (K)

T_s: Shell side temperature (K)

 T_t : Fiber side temperature (K)

 x_i : Mole fraction of component i in the feed side

 y_i : Mole fraction of i in the fiber side of the membrane

N: Number of components

δ: Thickness of the membrane (m)

μ: Viscosity of components on the fiber side (KPa. s)

 $1 = CO_2$; $2 = CH_4$; $3 = C_2H_4$; $4 = C_3$

References:

- [1] MTR Inc., "Polyethylene production," [Online]. Available: https://www.mtrinc.com/ petrochemical/ polyethylene-production/. Accessed: Nov. 10, 2023.
- [2] Indorama, "Indorama Products & Services Plant & Technology website," [Online]. Available: https: //www.indoramaeleme.com/products-&services.php?id=28. Accessed: Nov. 4, 2022.
- [3] P. Polat and E. Ersoz, "PP, PE producers cut run rates across Asia as high costs hammer margins," ChemOrbis, Mar. 11, 2022. [Online]. Available: https://www.chemorbis.com/en/plastics-news/PP-PE-producers-cut-run-rates-across-Asia-as-highcosts-hammer-margins/2022/03/11/839. Accessed: Dec. 14, 2022.
- [4] M. Bozorg, B. Addis, V. Piccialli, Á. A. Ramírez-Santos, C. Castel, I. Pinnau, and E. Favre, "Polymeric membrane materials for nitrogen production from air: A process synthesis study," *Chemical Engineering Science*, vol. 207, pp. 1196-1213, 2019.
- [5] M. T. Ravanchi, T. Kaghazchi, and A. Kargari, "Application of membrane separation processes in petrochemical industry: a review," *Desalination*, vol. 235, no. 1-3, pp. 199-244, 2009.
- [6] Bernardo, "Petrochemical Industry and Membrane Operations," in *Encyclopedia of Membranes*, E. Drioli and L. Giorno, Eds. Springer, Berlin, Heidelberg, 2014. [Online]. Available: https://doi.org/10.1007/978-3-642-40872-41624-1

- [7] A. Iulianelli and E. Drioli, "Membrane engineering: Latest advancements in gas separation and pretreatment processes, petrochemical industry and refinery, and future perspectives in emerging applications," *Fuel Processing Technology*, vol. 206, p. 106464, 2020.
- [8] L. Gai, Y. Van Fan, P. S. Varbanov, and J. J. Klemeš, "Membrane Separation for Light Hydrocarbons Recovery in the Petrochemical Industry," in 2021 6th International Conference on Smart and Sustainable Technologies (SpliTech), Sep. 2021, pp. 1-5. IEEE.
- [9] S. Munirasu, M. A. Haija, and F. Banat, "Use of membrane technology for oil field and refinery produced water treatment—A review," *Process Safety and Environmental Protection*, vol. 100, pp. 183-202, 2016.
- [10] P. G. Santos, C. M. Scherer, A. G. Fisch, and M. A. S. Rodrigues, "Petrochemical wastewater treatment: Water recovery using membrane distillation," *Journal of Cleaner Production*, vol. 267, p. 121985, 2020.
- [11] U. Chadha, S. K. Selvaraj, S. V. Thanu, V. Cholapadath, A. M. Abraham, M. Manoharan, and V. Paramsivam, "A review of the function of using carbon nanomaterials in membrane filtration for contaminant removal from wastewater," *Materials Research Express*, vol. 9, no. 1, p. 012003, 2022.
- [12] E. Favre, "Polymeric membranes for gas separation," in *Comprehensive Membrane Science and Technology*, E. Drioli and L. Giorno, Eds., vol. II, pp. 155-212, 2017.
- [13] Air Liquide, "Advanced membrane technology for hydrogen purification and recovery," *Hydrogen Membrane Overview*, [Online]. Available: https://advancedseparations.airliquide.com/sites/a las/files/2016/11/28/alas_h2_brochure.pdf. Accessed: Nov. 9, 2022.
- [14] A. R. T. Cardoso, A. Ambrosi, M. Di Luccio, and D. Hotza, "Membranes for separation of CO2/CH4 at harsh conditions," *Journal of Natural Gas Science* and Engineering, vol. 98, p. 104388, 2022.
- [15] SLB, "Cynara H2S and CO2 separation membranes," Gas Treatment, [online]. Available: https://www.slb.com/products-andservices/innovating-in-oil-and-gas/wellproduction/processing-and-separation/gas-

- treatment/cynara-h2s-and-co2-separation-membranes. Accessed: Nov. 8, 2022.
- [16] Borsig, "Organic solvent nano-filtration (OSN): Low energy sustainable processing," *Borsig Membrane Technology GBMH*, [Online].
- [17] M. D. Guiver, M. Yahia, M. M. Dal-Cin, G. P. Robertson, S. S. Garakani, N. Du, and N. Tavajohi, "Macromolecules," vol. 53, no. 20, pp. 8951-8959, 2020. DOI: 10.1021/acs.macromol.0c01321.
- [18] R. Swaidan, R. P. Lively, and W. J. Koros, "Polymers of intrinsic microporosity (PIMs) for gas separation membranes: a review of permeability and selectivity trends," *Chemical Reviews*, vol. 121, no. 6, pp. 3266-3326, 2021.
- [19] P. Li, T. S. Chung, and D. R. Paul, "Gas sorption and permeation in PIM-1," *Journal of Membrane Science*, vol. 432, pp. 50-57, 2013. DOI: 10.1016/j.memsci.2013.01.009.
- [20] C. G. Bezzu, M. Carta, A. Tonkins, J. C. Jansen, P. Bernardo, F. Bazzarelli, and N. B. McKeown, "A spirobifluorene-based polymer of intrinsic microporosity with improved performance for gas separation," *Advanced Materials*, vol. 24, no. 44, pp. 5930-5933, 2012.
- [21] I. A. Helmersen, "Simulation, optimization and mathematical modelling of a hybrid membrane system for natural gas dehydration and CO2 removal," M.S. thesis, Dept. of Chem. Eng., Faculty of Natural Sci., Norwegian Univ. of Sci. and Technol., Jul. 2020.
- [22] R. W. Baker, Membrane Technology and Applications, 3rd ed. Hoboken, NJ, USA: John Wiley & Sons, 2012.
- [23] S. Saadi, I. S. Al-Mutaz, and K. Karim, Ethylene and Polyethylene Plants: Design, Operation, and Maintenance. Boca Raton, FL, USA: CRC Press, 2017.
- [24] National Institute of Standards and Technology (NIST), "NIST Chemistry WebBook," [Online]. Available: https://webbook.nist.gov/cgi/inchi?ID=C124389& Mask=1#Thermo-Gas. Accessed: Jun. 1, 2023.
- [25] A. W. Thornton, B. D. Freeman, and L. M. Robeson, "Polymer Gas Separation Membrane Database," [Online]. Available: https://membrane-australasia.org/polymer-gas-separation-membrane-database/. Accessed: Jun. 1, 2023.